PHOTONICS Research

Active control of EIT-like response in a symmetry-broken metasurface with orthogonal electric dipolar resonators

Ruisheng Yang,[1] Quanhong Fu,[1,3] Yuancheng Fan,[1] Weiqi Cai,[1] Kepeng Qiu,[2] Weihong Zhang,[2] and Fuli Zhang[1,4]

[1]Research & Development Institute in Shenzhen, Key Laboratory of Space Applied Physics and Chemistry, Ministry of Education, and Department of Applied Physics, School of Natural and Applied Sciences, Northwestern Polytechnical University, Xi'an 710072, China
[2]School of Mechanical Engineering, Northwestern Polytechnical University, Xi'an 710072, China
[3]e-mail: fuquanhong@nwpu.edu.cn
[4]e-mail: fuli.zhang@nwpu.edu.cn

Received 1 May 2019; revised 11 June 2019; accepted 2 July 2019; posted 3 July 2019 (Doc. ID 366517); published 7 August 2019

The active control of electromagnetic response in metamaterial and mutual coupling between resonant building blocks is of fundamental importance in realizing high-quality metamaterials. In this work, we propose and experimentally demonstrate the tunabilities of symmetry-broken metasurfaces made of orthogonal electric dipolar resonators. The metasurface with vertical and horizontal wires is integrated with a PIN diode for active control. It is found that the electromagnetically induced transparency (EIT)-like spectrum appears due to the destructive or constructive interferences between the two electric dipolar modes when the structural symmetry broken is introduced to the metasurface. Different from previous works on the EIT-like effect, there is only electric dipole response in our metasuface. The microscopic response of the metasurface is numerically calculated to illustrate the mode coupling between the orthogonal electric dipolar resonators. By applying temporal coupled-mode theory, the interaction between the electromagnetic wave and the symmetry-broken metasurface is described, and the characteristic parameters of the resonator system, which determine the electromagnetic response of the metasurface, are acquired.

https://doi.org/10.1364/PRJ.7.000955

1. INTRODUCTION

Electromagnetically induced transparency (EIT) is a coherent process in atomic physics due to the quantum interference between different excitation pathways from the ground state to the final state observed in three-level atomic systems, leading to a narrow transparency window within a wide absorption band [1]. The strong dispersion and its resulting slow light [2] are two of the most significant features of EIT, and they have important applications in low-loss slow-light devices. However, the realization of EIT requires a very extreme external environment, which greatly limits the practical application. With the fast development of metamaterials [3–14] and their two-dimensional counterpart, metasurfaces [15–25], artificial microstructures are utilized to imitate EIT [26–40]. However, most traditional metamaterials with the EIT-like effect usually operate in a narrow frequency band owing to their resonant feature, which tremendously limits their applications in optoelectronic devices. To improve the performance, some active constituents, such as active elements [41–43], graphene [44–48], phase change materials [49–52], semiconductive materials [53,54], and liquid metal [55], are incorporated into metamaterials to realize active control of the EIT-like effect. In this work, we propose and experimentally demonstrate the tunabilities of symmetry-broken metasurfaces made of orthogonal electric dipolar resonators. The metasurface with vertical and horizontal wires is integrated with a PIN diode for active/dynamic control of the EIT-like effect. We find that the EIT-like spectrum appears due to the destructive or constructive interferences between the two electric dipolar modes when introducing the broken structural symmetry to the metasurface. The microscopic response of the metasurface is numerically calculated and analyzed in detail to illustrate the mode coupling between the orthogonal electric dipolar resonators. Using the temporal coupled-mode theory (TCMT) [56,57], the transmission spectrum of the metasurface is predicted, and the characteristic parameters of the resonator system are retrieved via parameter fitting. By altering the bias voltage applied on the PIN diode, the tunable EIT-like effect and modulation function of the metasurface are examined.

2. DESIGNS

Figure 1(a) displays the schematic of the symmetry-broken metasurface, which is composed of a vertical wire as bright resonator and a horizontal wire as a dark resonator. The photograph of the fabricated sample is shown in Fig. 2(b). To achieve a tunable EIT-like effect, a PIN diode (SMP1345, Skyworks) is soldered at the center of the vertical wire and is biased through the copper wires. As the bias voltage varies from 0 to 1.2 V, the PIN diode switches from off to on, and the EIT-like effect of the symmetry-broken metasurface is dynamically tuned. The metallic pattern is fabricated using the standard printed circuit board (PCB) technology. In experiments, the scattering parameters of the metasurface are measured inside a standard rectangular waveguide of WR284, in which the TE_{10} mode with an electric field polarizing along the vertical wire is normally incident on the metasurface, and the parameters are recorded via using a vector network analyzer (AV3629D).

Figure 2(a) illustrates the simulated transmission spectra of the vertical wire alone (green curve), horizontal wire alone (blue curve), and the symmetry-broken metasurface (red curve) when the resistance of PIN diode is 2 Ω. The vertical wire couples strongly to the incident TE_{10} mode in the waveguide and is therefore a bright resonator. The electric dipole resonance of the vertical wire occurs at 3.05 GHz with a transmission dip of −25.32 dB. In the waveguide, the horizontal wire can neither be excited by the incident wave nor coupled to the far-field radiation, so it is a dark resonator, and its transmission spectrum is nearly a constant of 0 dB. It should be noted that the periodic repetition of the structure in free space will not exhibit a similar EIT-like effect because the horizontal wire couples to the far-field radiation of horizontal polarization and is not a dark element anymore. In the symmetry-broken metasurface, the interference between the bright and dark modes resembles that between two different excitation pathways from the ground state to the final state in a three-level EIT system as shown in Fig. 2(b). The two possible excitation pathways include $|0\rangle - |1\rangle$ and $|0\rangle - |1\rangle - |2\rangle - |1\rangle$, which correspond to the electric dipole excitation in the vertical wire excited by the incident wave and horizontal wire, respectively. Owing to the destructive interference between the bright and dark modes, the electric dipole scattering of the vertical wire is highly suppressed, and the EIT-like effect occurs with transmittance approaching −0.51 dB at 2.97 GHz. It is worth noting that the

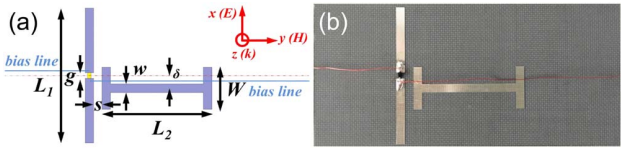

Fig. 1. (a) Schematic and (b) photograph of the symmetry-broken metasurface. The metallic pattern is copper with a conductivity of 5.8×10^7 S/m, and its depth is 0.035 mm. The 72.14 mm × 34.04 mm × 1.0 mm-substrate is Teflon with a relative permittivity of 2.65 and a loss tangent of 4×10^{-4}. The geometric parameters of the metasurface are as follows: $L_1 = 32$ mm, $L_2 = 26$ mm, $w = 2$ mm, $g = 1.3$ mm, $\delta = 3$ mm, $W = 10$ mm, and $s = 2$ mm. A PIN diode is located at the center of the vertical wire. Two bias copper wires indicated by sky blue lines have a diameter of 0.1 mm.

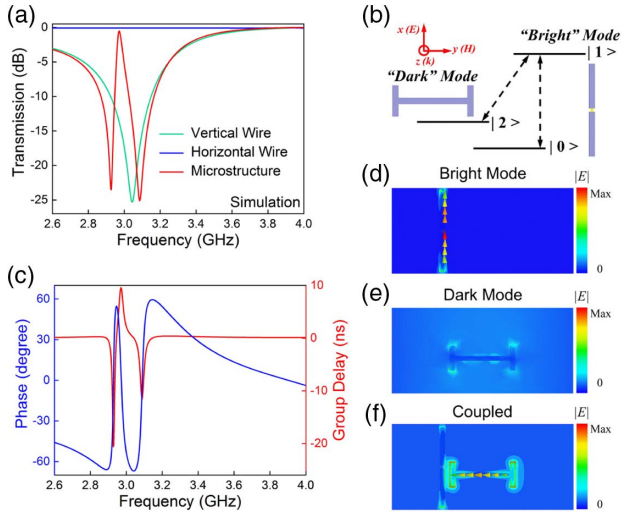

Fig. 2. (a) Simulated transmission spectra of the vertical wire alone (green curve), horizontal wire alone (blue curve), and the symmetry-broken metasurface (red curve). (b) Schematic view of destructive interference between the bright and dark modes. (c) Simulated transmission phase (blue curve) and group delay (red curve) of the symmetry-broken metasurface. (d)–(f) Distribution of the electric field on the plane where the metallic pattern is located and the induced surface current indicated by arrows on the metallic pattern at 2.97 GHz. All these results are obtained when the resistance of the PIN diode is 2 Ω.

EIT-like peak of our metasurface is quite sharp with a full width at half-maximum (FWHM) of 0.055 GHz, reaching a high quality factor of 54. Figure 2(c) shows the simulated transmission phase and group delay of the symmetry-broken metasurface. It can be seen that, around the EIT-like peak, the transmission phase decreases rapidly with frequency, resulting in a large group delay. It is significant that as the electromagnetic wave travels through the 0.035 mm thick metasurface, it experiences a maximum group delay of 9.6 ns around the EIT-like peak, corresponding to a 2.06 m long transmission line. The distribution of the electric field and the induced surface current shown in Figs. 2(d)–2(f) demonstrate that the electric dipole response of the vertical wire alone is much stronger than that of the horizontal wire alone, but the opposite is true in the symmetry-broken metasurface, confirming the destructive interference between the electric dipole modes of the orthogonal electric dipolar resonators.

3. RESULTS AND DISCUSSION

To quantitatively describe the interaction between the incident wave and the symmetry-broken metasurface, the TCMT is employed to analyze the mode coupling between the vertical and horizontal wires as well as the scattering parameters of the metasurface. According to the TCMT, the transmission spectrum of the metasurface excited by a monochromatic wave can be expressed as follows [43,56,57]:

$$t = \frac{(j\omega - j\omega_1 + \Gamma_{i1})(j\omega - j\omega_2 + \Gamma_{i2}) + \kappa^2}{(j\omega - j\omega_1 + \Gamma_{i1} + \Gamma_{e1})(j\omega - j\omega_2 + \Gamma_{i2}) + \kappa^2}, \quad (1)$$

where ω_1, Γ_{e1}, and Γ_{i1} (or ω_2, Γ_{e2}, and Γ_{i2}) represent the resonance frequency, radiative decay rate, and nonradiative decay rate of the bright (or dark) resonator, respectively, and κ denotes the direct coupling coefficient between the orthogonal electric dipolar resonators. The characteristic parameters of the resonator system can be obtained through fitting the expression of $|t|$ to the simulated transmission spectrum of the symmetry-broken metasurface shown in Fig. 2(a), as follows:

$$\begin{aligned}\omega_1 &= 2\pi \times 3.045 \times 10^9 \text{ rad/s},\\ \omega_2 &= 2\pi \times 2.975 \times 10^9 \text{ rad/s},\\ \Gamma_{e1} &= 2\pi \times 0.310 \times 10^9 \text{ rad/s},\\ \Gamma_{i1} &= 2\pi \times 0.018 \times 10^9 \text{ rad/s},\\ \Gamma_{i2} &= 2\pi \times 0.001 \times 10^9 \text{ rad/s},\\ \kappa &= 2\pi \times 0.074 \times 10^9 \text{ rad/s}.\end{aligned}$$

It is obvious that the values of ω_1 and ω_2 correspond to the transmission dip of the vertical wire alone and the transmission peak of the symmetry-broken metasurface, respectively, as shown in Fig. 2(a). For the vertical wire, the radiative decay rate Γ_{e1} is about 17 times larger than the nonradiative decay rate Γ_{i1}. The nonradiative decay rate of the horizontal wire Γ_{i2} is much less than that of the vertical wire Γ_{i1}, and it is therefore negligible. It is significant that the frequency interval between the two transmission dips of the symmetry-broken metasurface is merely 0.16 GHz, because the direct coupling coefficient κ is much less than the resonance frequencies, ω_1 and ω_2, and even the radiative decay rate Γ_{e1}. The TCMT accurately predicts the transmission spectrum of the symmetry-broken metasurface as shown in Fig. 3(a), indicating that the TCMT exactly describes the mode coupling between the orthogonal electric dipolar resonators.

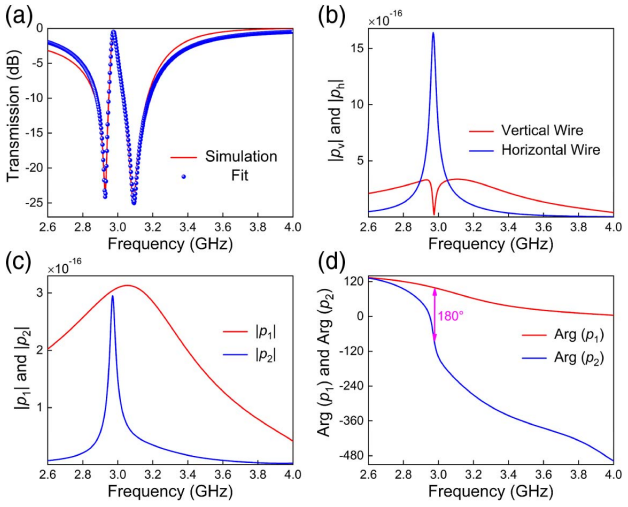

Fig. 3. (a) Transmission spectra of the symmetry-broken metasurface predicted by the TCMT (blue points) and simulated through FEM (red curve). (b) Magnitude of the electric dipole moment of vertical wire (p_v, red curve) and horizontal wire (p_h, blue curve) in the symmetry-broken metasurface. (c) Magnitude and (d) phase of p_1 and p_2. All these results are obtained when the resistance of the PIN diode is 2 Ω.

To further interpret the coupling mechanism between the orthogonal electric dipolar resonators as well as the scattering feature of the symmetry-broken metasurface, the microscopic response, i.e., electric dipole moment, of the vertical and horizontal wires, p_v and p_h, is analyzed through full-wave simulation and numerical calculation. Figure 3(b) shows the spectra of the electric dipole moment of the vertical and horizontal wires. It is seen that, around the EIT-like peak, a dip with minimum close to zero but not exactly equal to zero appears in the magnitude spectrum of electric dipole moment of the vertical wire, while the magnitude of the electric dipole moment of the horizontal wire reaches maximum, indicating that the electric dipole response of the vertical wire is strongly suppressed by the horizontal wire via near-field coupling. Note that the horizontal electric dipole does not radiate because the proposed structure is placed inside a standard rectangular waveguide where only the fundamental mode, i.e., TE_{10} mode, can propagate in the frequency range of interest. The electric field of the TE_{10} mode polarizes along x axis, so only the electric dipole with a direction parallel to x axis can radiate into the far field, and the electric dipole with direction parallel to the y or z axis cannot radiate into the far field. Since the horizontal wire does not have radiative loss and its nonradiative loss is negligible, the spectrum of the electric dipole moment in the horizontal wire excited by the unit electric dipole moment in the vertical wire has an extremely high quality factor, and the weak electric dipole moment in the vertical wire excites the strong electric dipole moment in the horizontal wire around the EIT-like peak.

In the symmetry-broken metasurface, the electric dipole moment of the vertical wire p_v can be divided into two parts, p_1 and p_2. p_1 is the electric dipole moment of the vertical wire excited by the incident field of TE_{10} mode, which is the analogy of the excitation pathway of $|0\rangle - |1\rangle$ shown in Fig. 2(b), while p_2 is the electric dipole moment of the vertical wire excited by the near field of the horizontal wire, which corresponds to the excitation pathway of $|0\rangle - |1\rangle - |2\rangle - |1\rangle$ shown in Fig. 2(b). The electric dipole moment can be calculated from the induced surface current according to the following formula:

$$p = \frac{1}{j\omega}\int j_S(x)\mathrm{d}S. \tag{2}$$

p_v is calculated in the presence of the horizontal wire; p_1 is calculated in the absence of the horizontal wire; p_2 is calculated by subtracting p_1 from p_v.

Figures 3(c) and 3(d) exhibit the magnitude and phase of p_1 and p_2, respectively. It is evident that p_1 is a broadband resonance owing to the large radiative loss of the vertical wire, while p_2 is a narrowband resonance because of the narrowband excitation source, i.e., the electric dipole moment of the horizontal wire, p_h, indicated by the blue curve in Fig. 3(b). Distinct from the phase variation of p_1, the phase of p_2 varies with frequency rapidly because of the weak coupling between the vertical and horizontal wires, leading to narrow frequency interval between the two transmission dips. Around the EIT-like peak, the phase difference between p_2 and p_1 is 180°, and the magnitude of p_2 approaches that of p_1, which further confirms the destructive interference effect in the symmetry-broken metasurface and explains the origin of the high transmittance.

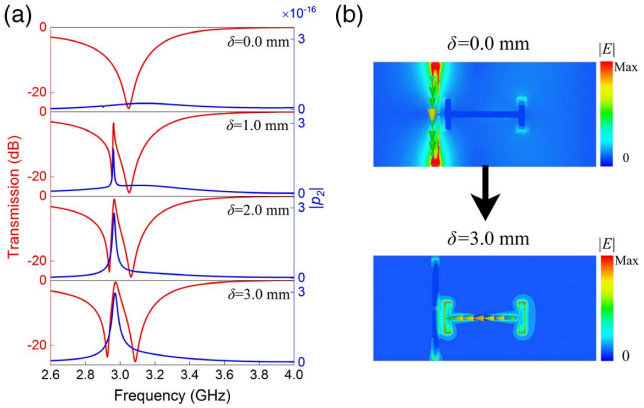

Fig. 4. (a) Simulated transmission spectra of the symmetry-broken metasurface and calculated magnitude spectra of p_2, which represent the interaction between the vertical and horizontal wires for $\delta = 0$, 1.0, 2.0, and 3.0 mm. (b) Distribution of the electric field on the plane where the metallic pattern is located as δ varies from 0 to 3 mm at 2.97 GHz. All these results are obtained when the resistance of the PIN diode is 2 Ω.

Moreover, it is significant that the magnitude of p_b is nearly 5 times larger than that of p_1, implying that the localized field enhancement effects of the dark resonator is much more prominent than that of the bright resonator alone.

The asymmetry of the metasurface is crucial to the occurrence of the EIT-like effect. When the metasurface is symmetric with $\delta = 0$ mm, the horizontal wire cannot be excited by the vertical wire, and thus the vertical wire is not coupled with the horizontal wire. As a result, the metasurface shows the electric dipole resonance of the vertical wire. However, when $\delta > 0$ mm, the horizontal wire can be excited by the parallel electric field component of the near field of the vertical wire, and the EIT-like spectrum appears due to the mode coupling between the orthogonal electric dipolar resonators. Figure 4(a) demonstrates the influence of the asymmetry δ on the electromagnetic response of the metasurface and the interaction between the vertical and horizontal wires. When $\delta = 0$ mm, the electric dipole moment of the vertical wire excited by the horizontal wire, p_2, is negligible and the vertical wire behaves as if the horizontal wire does not exist. With the increment of δ, the magnitude of p_2 gradually increases and the bandwidth of p_2 broadens, so the transmittance at the transmission peak grows higher and the frequency interval between the two transmission dips increases. The distributions of the electric field as well as the induced surface current at the transmission peak frequency of 2.97 GHz are shown in Fig. 4(b). When located at the center of the cross section of the waveguide, the horizontal wire cannot be excited while the vertical wire is strongly coupled with the incident wave. After introducing symmetry breaking, the horizontal wire can be excited by the vertical wire and in turn highly suppresses the electric dipole response of the vertical wire.

In what follows, the dynamic control of electric dipole resonance in the vertical wire alone integrated with the PIN diode is investigated first. Figure 5(a) presents the measured transmission spectra of the vertical wire alone on substrate with the bias voltage ranging from 0 to 1.2 V. It can be seen that the high bias voltage has opposite influence on the transmission

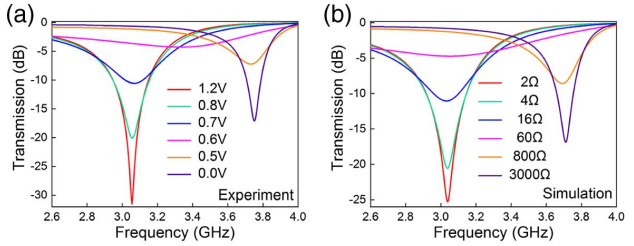

Fig. 5. (a) Measured and (b) simulated transmission spectra of the vertical wire alone on substrate with the bias voltage ranging from 0 to 1.2 V, and accordingly the resistance of the PIN diode varying from 3000 Ω to 2 Ω.

spectrum compared with the low bias voltage. Under high bias voltage, for example above 0.7 V, the PIN diode is metallic, and hence the vertical wire is unbroken, so the electric dipole resonance occurs at lower frequencies; when the bias voltage is 1.2 V, the electric dipole resonance occurs at 3.06 GHz with transmittance of −31.48 dB, which is the metallic limit of the vertical wire; as the bias voltage drops from 1.2 to 0.7 V and the resistance of PIN diode increases, the loss increases but the resonance frequency is almost constant, so the electric dipole resonance weakens and the bandwidth broadens, resulting in the decrease of quality factor. Nevertheless, under low bias voltage, for example below 0.5 V, the PIN diode is dielectric, and thus the vertical wire is broken, so the electric dipole resonance occurs at higher frequencies; when the bias voltage is 0 V, the electric dipole resonance occurs at 3.75 GHz with transmittance of −17.10 dB, which is the dielectric limit of vertical wire; as the bias voltage drops from 0.5 to 0 V and the resistance of PIN diode increases, the loss decreases and the resonance frequency is nearly unchanged, so the electric dipole resonance is enhanced and the bandwidth becomes narrow, leading to an increase in quality factor. Note that the case of 0.6 V is an intermediate state between the metallic and dielectric states and has the highest loss. The simulated results shown in Fig. 5(b) agree well with the experimental results, verifying the effective manipulation of loss and even frequency of electric dipole resonance by the PIN diode.

The tunable EIT-like effect of the symmetry-broken metasurface is also investigated. Figure 6(a) shows the measured transmission spectra of the metasurface with the bias voltage ranging from 0 to 1.2 V.

Similar to the aforementioned case of vertical wire, the high bias voltage has different influence on the transmission spectrum

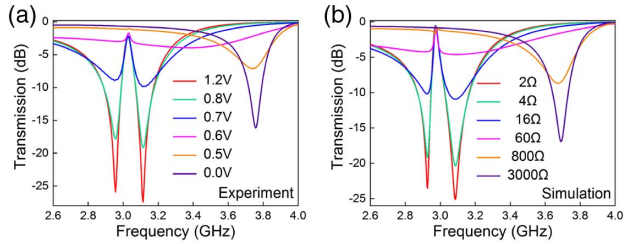

Fig. 6. Transmission spectra of the symmetry-broken metasurface obtained through both (a) experiment and (b) simulation with the bias voltage ranging from 0 to 1.2 V, and accordingly the resistance of the PIN diode varying from 3000 Ω to 2 Ω.

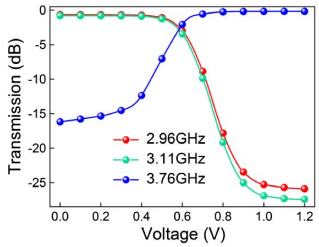

Fig. 7. Measured transmittance of the symmetry-broken metasurface versus the bias voltage at 2.96 GHz (red curve), 3.11 GHz (green curve), and 3.76 GHz (blue curve).

compared with the low bias voltage for the symmetry-broken metasurface. Under high bias voltage, for example above 0.7 V, the vertical wire is unbroken, and its resonance frequency is close to that of horizontal wire, so the vertical wire is coupled with the horizontal wire and the metasurface shows the EIT-like effect; when the bias voltage is 1.2 V, the transmittance at the two transmission dips, i.e., 2.96 and 3.11 GHz, is −25.89 dB and −27.41 dB, respectively, which is the metallic limit of the metasurface; as the bias voltage drops from 1.2 to 0.7 V and the resistance of PIN diode increases, the transmittance at both of the two transmission dips increases because the electric dipole resonance of vertical wire weakens, but the transmittance at the transmission peak is almost unchanged. However, under low bias voltage, for example, below 0.5 V, the vertical wire is broken, and its resonance frequency is far from that of horizontal wire, so the horizontal wire does not work, and the metasurface shows the electric dipole resonance of vertical wire; as the bias voltage drops from 0.5 to 0 V and the resistance of PIN diode increases, the variation of transmission spectrum of the metasurface is the same as the aforementioned case of vertical wire. The case of 0 V is the dielectric limit of the metasurface, and the case of around 0.6 V remains the intermediate state between the metallic and dielectric states of the metasurface. The simulated results demonstrated in Fig. 6(b) match well with the experimental results, verifying the effective manipulation of the EIT-like effect by the PIN diode.

In Fig. 6, it is worth noting that the transmittance of the symmetry-broken metasurface undergoes remarkable changes at specific frequencies as the bias voltage ranges from 0 to 1.2 V, enabling the application of the metasurface as an amplitude modulator. To illustrate the amplitude modulation capability of the metasurface, the variation of measured transmittance with bias voltage for microwaves at 2.96, 3.11, and 3.76 GHz is displayed in Fig. 7. When the bias voltage varies from 0 to 1.2 V, the transmittance monotonously decreases from −0.65 to −25.89 dB at 2.96 GHz, demonstrating a modulation depth of 95%, and similar modulation feature is shown at 3.11 GHz; nevertheless, the transmittance monotonously increases from −16.18 to −0.16 dB at 3.76 GHz, demonstrating a modulation depth of 84%. Hence, the symmetry-broken metasurface can act as a triple-band amplitude modulator.

4. CONCLUSION

In conclusion, we have presented a symmetry-broken metasurface integrated with a PIN diode and investigated the electrically controlled EIT-like effect via both experiments and simulations. After introducing asymmetry into the metasurface, the vertical wire is coupled with the horizontal wire, and the EIT-like effect occurs due to the destructive interference between the two electric dipole modes. Utilizing the TCMT, the characteristic parameters of the resonator system are acquired and the transmission spectrum of the metasurface is exactly reproduced. The analysis of microscopic response of the metasurface further demonstrates the underlying physics of the EIT-like effect. We also found that the transmittance around the transmission dips of the metasurface undergoes a remarkable change via controlling the bias voltage applied on the PIN diode. This work is promising in the application of multi-frequency microwave modulating and signal processing.

Funding. National Natural Science Foundation of China (NSFC) (11372248, 11674266, 61505164, 61771402); Natural Science Foundation of Shaanxi Province (2017JM6094, 2017JQ5116, 2018JM6024); Shenzhen Science and Technology Innovation Commission (JCYJ20170817162221169); Fundamental Research Funds for the Central Universities (3102017zy033, 3102018jgc008, 3102018zy045); Society of Hong Kong Scholars (XJ2017006).

REFERENCES

1. S. E. Harris, "Electromagnetically induced transparency," Phys. Today **50**, 36–42 (1997).
2. L. V. Hau, S. E. Harris, Z. Dutton, and C. H. Behroozi, "Light speed reduction to 17 metres per second in an ultracold atomic gas," Nature **397**, 594–598 (1999).
3. J. B. Pendry, "Negative refraction makes a perfect lens," Phys. Rev. Lett. **85**, 3966–3969 (2000).
4. R. A. Shelby, D. R. Smith, and S. Schultz, "Experimental verification of a negative index of refraction," Science **292**, 77–79 (2001).
5. S. Linden, C. Enkrich, M. Wegener, J. F. Zhou, T. Koschny, and C. M. Soukoulis, "Magnetic response of metamaterials at 100 terahertz," Science **306**, 1351–1353 (2004).
6. J. B. Pendry, "A chiral route to negative refraction," Science **306**, 1353–1355 (2004).
7. H. T. Chen, W. J. Padilla, J. M. O. Zide, A. C. Gossard, A. J. Taylor, and R. D. Averitt, "Active terahertz metamaterial devices," Nature **444**, 597–600 (2006).
8. N. I. Landy, S. Sajuyigbe, J. J. Mock, D. R. Smith, and W. J. Padilla, "Perfect metamaterial absorber," Phys. Rev. Lett. **100**, 207402 (2008).
9. J. K. Gansel, M. Thiel, M. S. Rill, M. Decker, K. Bade, V. Saile, G. von Freymann, S. Linden, and M. Wegener, "Gold helix photonic metamaterial as broadband circular polarizer," Science **325**, 1513–1515 (2009).
10. Q. Zhao, J. Zhou, F. L. Zhang, and D. Lippens, "Mie resonance-based dielectric metamaterials," Mater. Today **12**, 60–69 (2009).
11. N. Liu, M. Hentschel, T. Weiss, A. P. Alivisatos, and H. Giessen, "Three-dimensional plasmon rulers," Science **332**, 1407–1410 (2011).
12. N. K. Grady, J. E. Heyes, D. R. Chowdhury, Y. Zeng, M. T. Reiten, A. K. Azad, A. J. Taylor, D. A. R. Dalvit, and H. T. Chen, "Terahertz metamaterials for linear polarization conversion and anomalous refraction," Science **340**, 1304–1307 (2013).
13. S. Jahani and Z. Jacob, "All-dielectric metamaterials," Nat. Nanotechnol. **11**, 23–36 (2016).
14. Y. Fan, N. H. Shen, F. Zhang, Q. Zhao, H. Wu, Q. Fu, Z. Wei, H. Li, and C. M. Soukoulis, "Graphene plasmonics: a platform for 2D optics," Adv. Opt. Mater. **7**, 1800537 (2019).
15. N. F. Yu, P. Genevet, M. A. Kats, F. Aieta, J. P. Tetienne, F. Capasso, and Z. Gaburro, "Light propagation with phase discontinuities: generalized laws of reflection and refraction," Science **334**, 333–337 (2011).

16. S. Sun, Q. He, S. Xiao, Q. Xu, X. Li, and L. Zhou, "Gradient-index meta-surfaces as a bridge linking propagating waves and surface waves," Nat. Mater. **11**, 426–431 (2012).
17. S. Sun, K. Y. Yang, C. M. Wang, T. K. Juan, W. T. Chen, C. Y. Liao, Q. He, S. Xiao, W. T. Kung, G. Y. Guo, L. Zhou, and D. P. Tsai, "High-efficiency broadband anomalous reflection by gradient meta-surfaces," Nano Lett. **12**, 6223–6229 (2012).
18. X. B. Yin, Z. L. Ye, J. Rho, Y. Wang, and X. Zhang, "Photonic spin Hall effect at metasurfaces," Science **339**, 1405–1407 (2013).
19. L. Liu, X. Zhang, M. Kenney, X. Su, N. Xu, C. Ouyang, Y. Shi, J. Han, W. Zhang, and S. Zhang, "Broadband metasurfaces with simultaneous control of phase and amplitude," Adv. Mater. **26**, 5031–5036 (2014).
20. N. Yu and F. Capasso, "Flat optics with designer metasurfaces," Nat. Mater. **13**, 139–150 (2014).
21. A. Arbabi, Y. Horie, M. Bagheri, and A. Faraon, "Dielectric metasurfaces for complete control of phase and polarization with subwavelength spatial resolution and high transmission," Nat. Nanotechnol. **10**, 937–943 (2015).
22. M. Decker, I. Staude, M. Falkner, J. Dominguez, D. N. Neshev, I. Brener, T. Pertsch, and Y. S. Kivshar, "High-efficiency dielectric Huygens' surfaces," Adv. Opt. Mater. **3**, 813–820 (2015).
23. H. T. Chen, A. J. Taylor, and N. Yu, "A review of metasurfaces: physics and applications," Rep. Prog. Phys. **79**, 076401 (2016).
24. S. B. Glybovski, S. A. Tretyakov, P. A. Belov, Y. S. Kivshar, and C. R. Simovski, "Metasurfaces: from microwaves to visible," Phys. Rep. **634**, 1–72 (2016).
25. M. Khorasaninejad, W. T. Chen, R. C. Devlin, J. Oh, A. Y. Zhu, and F. Capasso, "Metalenses at visible wavelengths: diffraction-limited focusing and subwavelength resolution imaging," Science **352**, 1190–1194 (2016).
26. N. Papasimakis, V. A. Fedotov, N. I. Zheludev, and S. L. Prosvirnin, "Metamaterial analog of electromagnetically induced transparency," Phys. Rev. Lett. **101**, 253903 (2008).
27. S. Zhang, D. A. Genov, Y. Wang, M. Liu, and X. Zhang, "Plasmon-induced transparency in metamaterials," Phys. Rev. Lett. **101**, 047401 (2008).
28. N. Liu, L. Langguth, T. Weiss, J. Kastel, M. Fleischhauer, T. Pfau, and H. Giessen, "Plasmonic analogue of electromagnetically induced transparency at the Drude damping limit," Nat. Mater. **8**, 758–762 (2009).
29. N. Papasimakis, Y. H. Fu, V. A. Fedotov, S. L. Prosvirnin, D. P. Tsai, and N. I. Zheludev, "Metamaterial with polarization and direction insensitive resonant transmission response mimicking electromagnetically induced transparency," Appl. Phys. Lett. **94**, 211902 (2009).
30. R. Singh, C. Rockstuhl, F. Lederer, and W. L. Zhang, "Coupling between a dark and a bright eigenmode in a terahertz metamaterial," Phys. Rev. B **79**, 085111 (2009).
31. P. Tassin, L. Zhang, T. Koschny, E. N. Economou, and C. M. Soukoulis, "Low-loss metamaterials based on classical electromagnetically induced transparency," Phys. Rev. Lett. **102**, 053901 (2009).
32. P. Tassin, L. Zhang, T. Koschny, E. N. Economou, and C. M. Soukoulis, "Planar designs for electromagnetically induced transparency in metamaterials," Opt. Express **17**, 5595–5605 (2009).
33. S.-Y. Chiam, R. Singh, C. Rockstuhl, F. Lederer, W. Zhang, and A. A. Bettiol, "Analogue of electromagnetically induced transparency in a terahertz metamaterial," Phys. Rev. B **80**, 153103 (2009).
34. Z.-G. Dong, H. Liu, J.-X. Cao, T. Li, S.-M. Wang, S.-N. Zhu, and X. Zhang, "Enhanced sensing performance by the plasmonic analog of electromagnetically induced transparency in active metamaterials," Appl. Phys. Lett. **97**, 114101 (2010).
35. N. Liu, T. Weiss, M. Mesch, L. Langguth, U. Eigenthaler, M. Hirscher, C. Sonnichsen, and H. Giessen, "Planar metamaterial analogue of electromagnetically induced transparency for plasmonic sensing," Nano Lett. **10**, 1103–1107 (2010).
36. C. Kurter, P. Tassin, L. Zhang, T. Koschny, A. P. Zhuravel, A. V. Ustinov, S. M. Anlage, and C. M. Soukoulis, "Classical analogue of electromagnetically induced transparency with a metal-superconductor hybrid metamaterial," Phys. Rev. Lett. **107**, 043901 (2011).
37. P. Tassin, L. Zhang, R. Zhao, A. Jain, T. Koschny, and C. M. Soukoulis, "Electromagnetically induced transparency and absorption in metamaterials: the radiating two-oscillator model and its experimental confirmation," Phys. Rev. Lett. **109**, 187401 (2012).
38. X. J. Liu, J. Q. Gu, R. Singh, Y. F. Ma, J. Zhu, Z. Tian, M. X. He, J. G. Han, and W. L. Zhang, "Electromagnetically induced transparency in terahertz plasmonic metamaterials via dual excitation pathways of the dark mode," Appl. Phys. Lett. **100**, 131101 (2012).
39. F. L. Zhang, Q. Zhao, J. Zhou, and S. X. Wang, "Polarization and incidence insensitive dielectric electromagnetically induced transparency metamaterial," Opt. Express **21**, 19675–19680 (2013).
40. Y. Yang, I. I. Kravchenko, D. P. Briggs, and J. Valentine, "All-dielectric metasurface analogue of electromagnetically induced transparency," Nat. Commun. **5**, 5753 (2014).
41. Q. Fu, F. Zhang, Y. Fan, X. He, T. Qiao, and B. Kong, "Electrically tunable Fano-type resonance of an asymmetric metal wire pair," Opt. Express **24**, 11708–11715 (2016).
42. Y. Fan, T. Qiao, F. Zhang, Q. Fu, J. Dong, B. Kong, and H. Li, "An electromagnetic modulator based on electrically controllable metamaterial analogue to electromagnetically induced transparency," Sci. Rep. **7**, 40441 (2017).
43. Q. Fu, F. Zhang, Y. Fan, J. Dong, W. Cai, W. Zhu, S. Chen, and R. Yang, "Weak coupling between bright and dark resonators with electrical tunability and analysis based on temporal coupled-mode theory," Appl. Phys. Lett. **110**, 221905 (2017).
44. H. Cheng, S. Q. Chen, P. Yu, X. Y. Duan, B. Y. Xie, and J. G. Tian, "Dynamically tunable plasmonically induced transparency in periodically patterned graphene nanostrips," Appl. Phys. Lett. **103**, 203112 (2013).
45. Y. Fan, N.-H. Shen, T. Koschny, and C. M. Soukoulis, "Tunable terahertz meta-surface with graphene cut-wires," ACS Photon. **2**, 151–156 (2015).
46. Y. Fan, N.-H. Shen, F. Zhang, Z. Wei, H. Li, Q. Zhao, Q. Fu, P. Zhang, T. Koschny, and C. M. Soukoulis, "Electrically tunable Goos-Hänchen effect with graphene in the terahertz regime," Adv. Opt. Mater. **4**, 1824–1828 (2016).
47. S. Y. Xiao, T. Wang, T. T. Liu, X. C. Yan, Z. Li, and C. Xu, "Active modulation of electromagnetically induced transparency analogue in terahertz hybrid metal-graphene metamaterials," Carbon **126**, 271–278 (2018).
48. Y. Fan, N.-H. Shen, F. Zhang, Q. Zhao, Z. Wei, P. Zhang, J. Dong, Q. Fu, H. Li, and C. M. Soukoulis, "Photoexcited graphene metasurfaces: significantly enhanced and tunable magnetic resonances," ACS Photon. **5**, 1612–1618 (2018).
49. E. Petronijevic and C. Sibilia, "All-optical tuning of EIT-like dielectric metasurfaces by means of chalcogenide phase change materials," Opt. Express **24**, 30411–30420 (2016).
50. W. Zhu, R. Yang, Y. Fan, Q. Fu, H. Wu, P. Zhang, N. H. Shen, and F. Zhang, "Controlling optical polarization conversion with $Ge_2Sb_2Te_5$-based phase-change dielectric metamaterials," Nanoscale **10**, 12054–12061 (2018).
51. J. Tian, H. Luo, Y. Yang, F. Ding, Y. Qu, D. Zhao, M. Qiu, and S. I. Bozhevolnyi, "Active control of anapole states by structuring the phase-change alloy $Ge_2Sb_2Te_5$," Nat. Commun. **10**, 396 (2019).
52. B. Gholipour, A. Karvounis, J. Yin, C. Soci, K. F. MacDonald, and N. I. Zheludev, "Phase-change-driven dielectric-plasmonic transitions in chalcogenide metasurfaces," NPG Asia Mater. **10**, 533–539 (2018).
53. J. Q. Gu, R. Singh, X. J. Liu, X. Q. Zhang, Y. F. Ma, S. Zhang, S. A. Maier, Z. Tian, A. K. Azad, H. T. Chen, A. J. Taylor, J. G. Han, and W. L. Zhang, "Active control of electromagnetically induced transparency analogue in terahertz metamaterials," Nat. Commun. **3**, 1151 (2012).
54. R. Yahiaoui, M. Manjappa, Y. K. Srivastava, and R. Singh, "Active control and switching of broadband electromagnetically induced transparency in symmetric metadevices," Appl. Phys. Lett. **111**, 021101 (2017).
55. J. Xu, Y. Fan, R. Yang, Q. Fu, and F. Zhang, "Realization of switchable EIT metamaterial by exploiting fluidity of liquid metal," Opt. Express **27**, 2837–2843 (2019).
56. S. H. Fan, W. Suh, and J. D. Joannopoulos, "Temporal coupled-mode theory for the Fano resonance in optical resonators," J. Opt. Soc. Am. A **20**, 569–572 (2003).
57. W. Suh, Z. Wang, and S. H. Fan, "Temporal coupled-mode theory and the presence of non-orthogonal modes in lossless multimode cavities," IEEE J. Quantum Electron. **40**, 1511–1518 (2004).